Applied Materials Today 18 (2020) 100496

Contents lists available at ScienceDirect

Applied Materials Today

journal homepage: www.elsevier.com/locate/apmt

Surface charge density of triboelectric nanogenerators: Theoretical boundary and optimization methodology

Chunlei Zhang[a,b,1], Linglin Zhou[a,b,1], Ping Cheng[a,b,1], Xing Yin[a,b], Di Liu[a,b], Xinyuan Li[a,b], Hengyu Guo[a,b], Zhong Lin Wang[a,b,c,*], Jie Wang[a,b,*]

[a] Beijing Institute of Nanoenergy and Nanosystems, Chinese Academy of Sciences, Beijing 100083, China
[b] College of Nanoscience and Technology, University of Chinese Academy of Sciences, Beijing 100049, China
[c] School of Materials Science and Engineering, Georgia Institute of Technology, Atlanta, GA 30332, USA

ARTICLE INFO

Article history:
Received 14 August 2019
Received in revised form
26 September 2019
Accepted 2 November 2019

Keywords:
Triboelectric nanogenerators
Mechanical energy harvesting
Charge decay
Charge accumulation
Thin dielectric layer

ABSTRACT

Although high charge densities of triboelectric nanogenerators (TENG) were achieved by working in high vacuum or charge pumping techniques in atmosphere, owing to their complex structure and/or stability issues, it still remains a great challenge and necessity to directly obtain the high charge density directly through triboelectrification effect in atmosphere. Here, a basic theory about the limitation factors of surface charge density is comprehensively rebuilt through analytical mathematical derivation of the limitation equation. As a result, high surface charge density can be obtained directly by a new optimization methodology, i.e. using thin dielectric layer, which is demonstrated by the designed contact-separation model TENG and sliding model TENG. In addition, the theoretical models of charge decay and charge accumulation during triboelectrification process were built. This work provides not only a new facile and universal optimization methodology for TENG, but also a new insight in the triboelectrification process, both of which will prompt the applications of TENG ranging from powering electronic devices to harvesting large-scale blue energy.

1. Introduction

With a rapid development of small electronic devices in the past several decades, sustainably powering these uncountable devices with pollution-free energy sources has been becoming a severe issue [1,2]. To obtain a clean and sustainable power source, harvesting energy from ambient environment has been proven to be a promising strategy. As a new energy harvesting technology invented in 2012, triboelectric nanogenerator (TENG) has been demonstrated to efficiently harvest ubiquitous and constantly available mechanical energy and convert it into electricity. The working principle of TENG is based on the coupling effect of triboelectrification and electrostatic induction, and the fundamental theory lies in Maxwell's displacement current and change in surface polarization [3–9]. Based on the basic operating principle, various TENGs have been developed to harvest mechanical energy from different types of motion, like body motions, wind, and ocean waves [10–14]. Abundant researches on TENG have well confirmed its potential of wide application in not only powering small electronic devices as self-powered systems and working as active sensors, but also harvesting water wave energy in large-scale blue energy [15–19]. As an energy harvesting device, the further extensive application of TENGs needs to enhance its output power density, which has been demonstrated to be quadratically related to its surface charge density (σ_{sc}) [20,21]. Hence, lots of efforts have been focused on improving σ_{sc} by means of material choice, structural optimization, artificial ion injection and so on, where σ_{sc} was improved from 30 μC m^{-2} to 250 μC m^{-2} [20,22–27]. Nevertheless, their outputs were limited by the air avalanche breakdown according to Paschen's law [28]. To avoid the air breakdown, the TENG was operated in vacuum environment and a high charge density of 1003 μC m^{-2} was achieved [29]. Whereas, in most practical situations, TENGs are operating in the air atmosphere, where the maximum surface charge density (σ_m) has been still restricted because of the air breakdown effect. Very recently, high surface charge densities in atmosphere were achieved by an external-charge TENG pumper and a self-charge excitation TENG system, respectively [30–32]. However, owing to complex circuit structure and stable issue of these sys-

* Corresponding authors at: Beijing Institute of Nanoenergy and Nanosystems, Chinese Academy of Sciences, Beijing 100083, China.
E-mail addresses: zhong.wang@mse.gatech.edu (Z.L. Wang), wangjie@binn.cas.cn (J. Wang).
[1] These authors contributed equally to this work.

https://doi.org/10.1016/j.apmt.2019.100496
2352-9407/

tems, it still remains a great challenge and necessity to directly obtain the high output charge density only through triboelectrification effect and electrostatic induction effect in atmosphere until now.

In this work, a high surface charge density is realized in atmosphere by using an thin film as TENG dielectric layer. Firstly, we systematically and precisely analyzed the effects of dielectric thickness (d) and separation distance (x_{Sep}) on surface charge density of dielectric layer for the contact-separation TENG (CS-TENG) by mathematical derivation of the limitation equation. It is the first time to point out the available range of Paschen's law in TENG field. Though reducing the d, we obtain an high surface charge density of 1090 μC m^{-2} in atmosphere through ion injection on an thin 6 μm Kapton film, further demonstrate the suitability of avalanche breakdown model in thin dielectric layer and establish a charge interface recombination model to explain the following charge decay process. Furthermore, we attain stable values of 418 and 740 μC m^{-2} by using fluorinated ethylene propylene (FEP) film with a thickness of 15 μm via the accumulation process of the triboelectric charge by contact-separation model and sliding model TENG, respectively. This work not only reach a new milestone of triboelectric charge density in atmosphere and a new paradigm shift to improve the outputs of TENGs, but also provide some new insights into the triboelectrification process.

2. Results

2.1. Limitation factors of surface charge density

When the electrode and dielectric layer of CS-TENG separate, an extremely high electrostatic field will be built between their surfaces with opposite triboelectric charges, simulated by finite-element method (Fig. S1, 2 and Note 1). Through the classical electrodynamics derivation and by ignoring edge effect, the drop of voltage between the contact surfaces under the short-circuit condition can be derived as follow (Supplementary Note 2) [26]:

$$V_{gap} = \frac{\sigma_0 dx}{\varepsilon_0(\mathrm{d} + \varepsilon_\mathrm{r}\mathrm{x})} \quad (1)$$

where σ_0 is the surface charge density of dielectric layer, d is the thickness of dielectric layer, x represents the gap distance, ε_0 and ε_r are the vacuum permittivity (8.85×10^{-12} F m^{-1}) and relative permittivity of dielectric layer, respectively. Theoretical analysis based on air breakdown voltage (V_b) described by the Paschen's law and the Eq. (1) can derive the relationship between the thickness (d) of the dielectric film on the maximum surface charge density (σ_m), named the limitation equation (Supplementary Note 3):

$$\sigma_m = \left(\frac{\mathrm{BP}\varepsilon_0(d + \varepsilon_r x)}{(\ln(Px) + C)d}\right)_{min} \quad (2)$$

where B and C are the constants determined by the composition and the pressure of the gas. For air at standard atmospheric pressure (P) of 101 kPa, they are 273.75 V Pa^{-1} m^{-1} and 1.08, respectively. It is found that the σ_m will increase with the decreasing of the d (Fig. 1a), which has been confirmed by previous reports [26]. For the CS-TENG based on Cu and polytetrafluoroethylene (PTFE), when the thickness of PTFE decreased from 600 to 200 μm in air, the charge density increased from 90 to 120 μC m^{-2} [25]. The value was further enhanced to 218.64 μC m^{-2} at fluorinated ethylene propylene (FEP) with thickness of 50 μm [20]. Additionally, the ion injection method for the introduction of surface charges on the FEP with different thickness was also carried out to obtain the corresponding σ_m. With the thickness of FEP decreasing from 125 to 50 μm, the charge density improved from 160 to 240 μC m^{-2} [22]. It can be found that both of the experimental values obtained from triboelectrification process and ion injection method agree well with the theoretical curve when the d exceeds 50 μm, which clearly illustrates that a thinner dielectric film is favorable for enhancing the surface charge density. However, the relationship between the σ_m and d of less than 50 μm was not confirmed through experiment to date. Besides, previous work focused on enhancing surface charges has verified that σ_m is

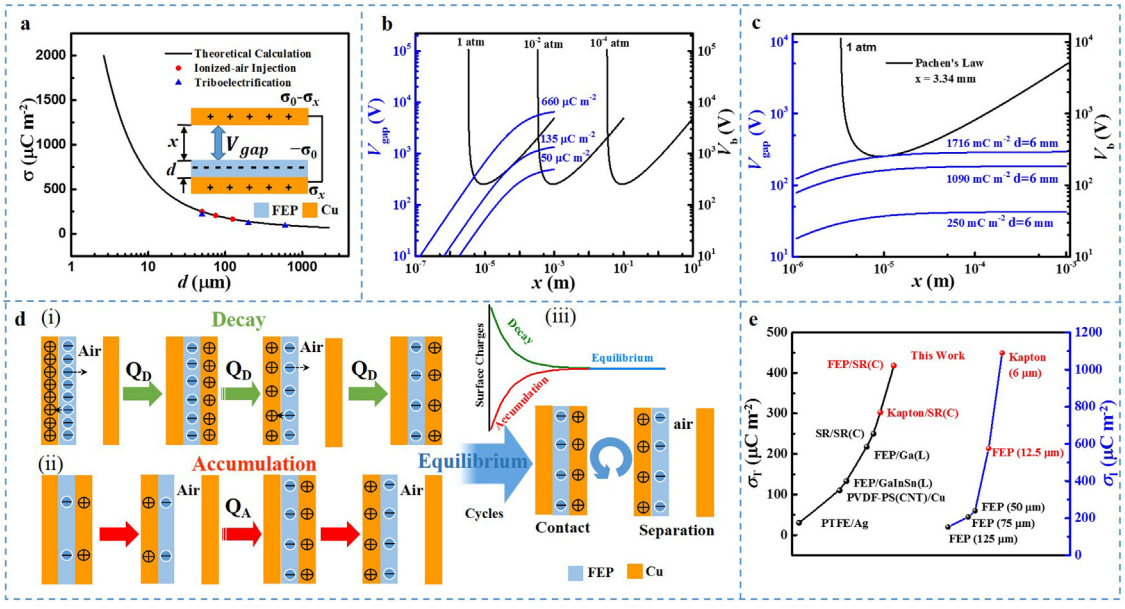

Fig. 1. Limitation factors of surface charge density. a) Theoretical analysis on the relationship between the maximum surface charge density (σ_m) and the thickness (d) of the FEP film in atmosphere, with the experimental data points of σ_m obtained for the d exceeding 50 μm.; b) Air breakdown voltage based on the Paschen's law and gap voltage of TENG with various charge densities, wherein PTFE film with thickness of 200 μm is used as the triboelectric material. c) Air breakdown voltage based on the Paschen's law at atmosphere and gap voltage of TENG between copper and an thin Kapton film of 6 μm with various charge densities. d) The simplified schematic diagram of charge accumulation and attenuation of TENGs. e) Comparison of the surface charge density measured in this work with that in previous works through the triboelectrification and the ion injection respectively, * means the value obtained by siding model TENG.

limited by air breakdown, which is almost inevitable in contact-separation TENG operating in atmosphere [28]. Recently, a high charge density in high vacuum is boosted to 660 μC m^{-2} with a Cu and PTFE [29], because V_{gap} in high vacuum (such as the pressure of 10^{-6} torr) is smaller than V_b with a general separation distance (1 cm), thereby avoiding the limitation of air breakdown (Fig. 1b). Whereas, σ_m of the TENG has been still limited to ~250 μC m^{-2} in the air atmosphere.

To avoid air breakdown, the V_{gap} must be smaller than V_b at any separation distance. Even if the surface charge density on the thin dielectric film (Kapton film, 6 μm) is up to an high value of 1716 μC m^{-2}, the V_{gap} is still not enough to break down the air between the gaps in theory (Fig. 1c). Therefore, the performance of TENGs at different thickness of Kapton and FEP film below 50 μm was studied and the results are presented in the following sections. Two points are of particular interest here. One is that an high surface charge density in atmosphere can be obtained through ion injection on thin dielectric films, but it decayed gradually. A charge interface recombination model is established to explain the surface charge decay process, where the surface charges may diffuse to atmosphere or the back electrode then result in a recombination with the opposite charges (Fig. 1d (i)). On the other hand, a stable and high surface charge density can be achieved in atmosphere by using thin dielectric film based on triboelectrification process and charge accumulation process (Fig. 1d (ii)). Then, a stable maximized output of TENG can be obtained when a dynamic equilibrium between charge accumulation and decay is built (Fig. 1d (iii)).

The significant stages in the development of TENG in air atmosphere are summarized (Fig. 1e). With the triboelectrification between Ag and PTFE, the surface charge density of TENG is around 30 μC m^{-2} at the beginning [18]. By introducing the electric double-layer effect and adding a charge transport layer, it can reach to 110 μC m^{-2} [19]. The value increases to 218.64 μC m^{-2} when liquid metal gallium replaced Cu as triboelectric electrode, due to better contact intimacy [20]. Inspired by liquid metal, we designed a soft material and fragmental contacting structure TENG to further enhance the surface charge density. The value is improved to 250 μC m^{-2}, approaching the limitation of air breakdown. In this work, a stable and high surface charge density of 418 μC m^{-2} and 735 μC m^{-2} is achieved in atmosphere by using FEP film with thickness of 15 μm via triboelectrification and surface charge accumulation process in contact-separate model TENG and sliding model TENG. Compared with that of the beginning TENG, the output triboelectric charge density has been boosted by 14-fold. Besides, using an thin Kapton film with the thickness of 6 μm, an high surface charge density of 1090 μC m^{-2} in atmosphere is realized through ion injection technique, which is 4 times as high as the value of 240 μC m^{-2} in previous work on the FEP film of 50 μm. The results indicate that a thinner dielectric film is favorable for achieving higher surface charge densities, which provides an optimized direction for designing the device of TENG and enhancing the surface charge density of TENG.

2.2. Theoretical maximum surface charge density

In previous work, the existence of air breakdown effect had been confirmed repeatedly. Once air breakdown occurs, immediate surface discharge on the dielectric layer will happen, resulting in a sharp decrease of dielectric surface charge density. Therefore, it's a dominant limitation of the output performance of TENG. The threshold voltage of air breakdown between two parallel plates follows the Paschen's law [24, 28] (Supplementary Note 3), which can be simplified as:

$$V_b = \frac{BPx}{\ln(Px) + C} \tag{3}$$

where B and C are the constants and which values are the same as the ones inEq. (2). It's apparent that V_b must be larger than zero, therefore,

$$\ln(\mathrm{P}x) + \mathrm{C} > 0 \tag{4}$$

Then, we can get the theoretical domain area of x >3.34 μm, which is consistent with the basic principle of Paschen's law. It was established on the theory of Townsend discharge, in which it's a result of avalanche multiplication that permits electrical conduction through the gas. The avalanche multiplication is a gas ionization process, wherein the free electrons are accelerated and then collided with gas molecules. So there will be a section of distance for the free electrons acceleration and a chain reaction in micron dimension. Through the above theoretical derivation, avalanche breakdown occurred where the gap distance (x_{gap}) must be greater than 3.34 μm.

It's obvious to note that σ_m depends on the x and d from limitation equation and then their three-dimension diagram can be plotted (Fig. 2a). Also the theoretical curve of σ_m for different thickness of thin FEP films below 50 μm is plotted based on the analysis above (Fig. 2b). To further obtain the quantitate mathematic relationship, we define the variable part of the limitation equation as a function *f(x,d)*:

$$f(x, d) = \frac{d + \varepsilon_{\mathrm{r}} x}{d(\ln(\mathrm{P}x) + \mathrm{C})} \tag{5}$$

Therefore,

$$\sigma_m = \mathrm{BP}\varepsilon_0 f(x, d)min \tag{6}$$

In order to obtain the minimum value of *f (x, d)*, it is necessary to take its partial derivatives for x and d respectively as following:

$$\frac{\partial f}{\partial x} = \frac{\varepsilon_{\mathrm{r}}(\ln(\mathrm{P}x) + \mathrm{C}) - (d + \varepsilon_{\mathrm{r}} x)\frac{1}{x}}{d(\ln(\mathrm{P}x) + \mathrm{C})^2} \tag{7}$$

$$\frac{\partial f}{\partial d} = -\frac{\varepsilon_{\mathrm{r}} x}{\ln(\mathrm{P}x) + \mathrm{C}} \cdot \frac{1}{d^2} \tag{8}$$

These equations indicate that the function *f(x,d)* increases first and then decreases in direction x, and monotonically decreases with d.

Then, set the $\partial f/\partial x$ =0, and we can get the following equation:

$$\varepsilon_{\mathrm{r}} x_E(\ln(\mathrm{P}x_E) + \mathrm{C} - 1) = d \tag{9}$$

The x_E is the gap distance in the case of $\partial f/\partial x = 0$, where the air breakdown is most likely to take place. From this equation, it can be found that x_E must be larger than 9.09 μm to satisfy $d > 0$ (Fig. 2b). In fact, the gap distance is generally larger than 1 cm in practical operation of CS-TENG.

According to the Eqs. (8) and (9), the maximum surface charge density can be obtained by the maximum surface charge density Eq. (10) or equation set (11, 12), while separation distance x_{Sep} is smaller or larger than x_E, respectively, (Supplementary Note 4):

$$\sigma_m = \frac{\mathrm{BP}\varepsilon_0(d + \varepsilon_{\mathrm{r}} x_{sep})}{(\ln(\mathrm{P}x_{sep}) + \mathrm{C})d} \; x_{sep} \in (3.34, x_E) \tag{10}$$

$$\sigma_m = \frac{\mathrm{BP}\varepsilon_0}{\ln(\mathrm{P}x_E) + \mathrm{C} - 1} \tag{11}$$

$$\varepsilon_{\mathrm{r}}\exp(\mathrm{BP}\varepsilon_0/\sigma_m + \ln(\mathrm{B}\varepsilon_0/\sigma_m) + 1 - \mathrm{C}) = d \; x_{sep} \in (x_E, +\infty) \tag{12}$$

With a certain d, σ_m shows a decreasing trend with the separation distance of CS-TENG increasing from 3.34 μm to x_E. We can see that the x_E is only 24 μm with the general FEP film of 50 μm. (Fig. 2c) For kapton dielectric layer, the relationship of σ_m between x_E and d is shown in Supplementary Fig. 3. Hence, a higher theoretical value of σ_m can be achieved when the micro separation distance

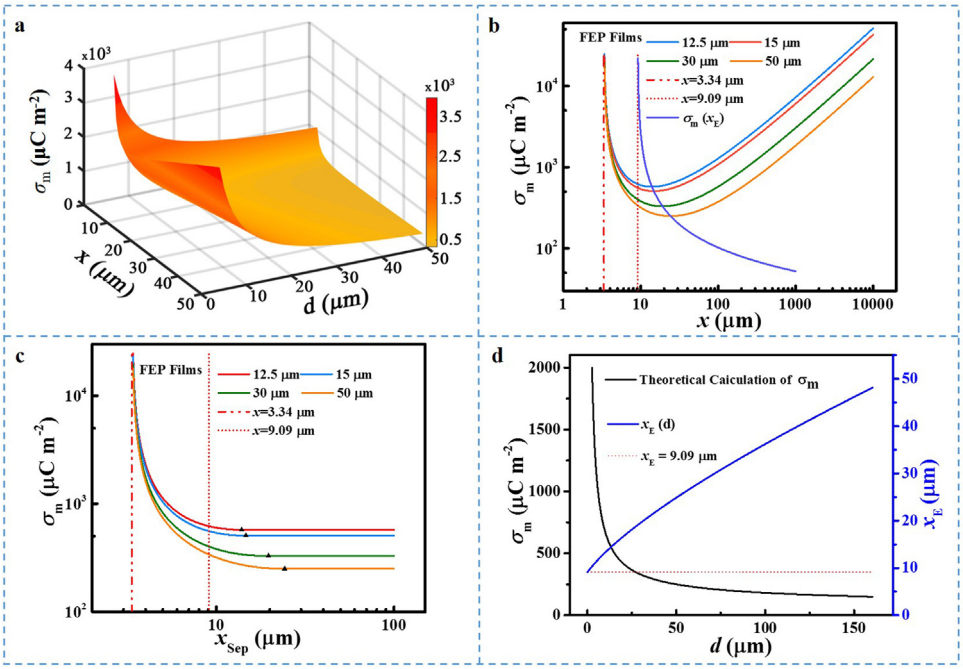

Fig. 2. Theoretical analysis of the performance of TENGs based on Paschen's law. a) The relationship plot among surface charge density, gap distance, and thickness of dielectric layer. b) The theoretical maximum surface charge density allowed without air breakdown of FEP films with thickness of 12.5, 15, 30 and 50 μm in various gap distances. c) The relationship between the σ_m of dielectric layer FEP with different thickness (12.5, 15, 30, and 50 μm) and the separation distance of TENG. d) The relationship between the dielectric layer thickness and the gap distance in the condition of $\partial(\sigma_0)_{max}/\partial x = 0$, and the relationship of theoretical maximum surface charge density and the thickness of dielectric layer.

smaller than x_E calculated from the Eq. (10). And as CS-TENG working with a micro dimension separation distance, the thin film is prerequisite to realize the approximately full transfer of electrons from front electrode to back electrode [33] (Supplementary Note 5). Once the separation distance is larger than the x_E, the occurrence of air breakdown will result in a constant σ_m which is determined by the d, which value can be calculated by Eq. (12).

Generally, after the d is given, the x_E and σ_m can be calculated from the Eqs. (9) and (12). According to the Eq. (12), it reveals that σ_m increases with the decreasing of d (Fig. 2d). It provides us an accurate way to estimate the theoretical limitation for different dielectric layer. Therefore, thinning the dielectric layer is an optimizing method to enhance the output performance of CE-TENG. Of course, the σ_m will be limited by dielectric layer breakdown or quantum tunneling effect in the case of thin dielectric layer.

2.3. Achieving maximum surface charge density via. ion injection method

The validity of relationship of σ_m and the d is confirmed in the case of d > 50 μm. Considering the features of triboelectrification and store charge are the key important factors for achieving high surface charge density of TENG, we choose the Kapton with high dielectric constant and FEP with high triboelectrification capacity to better study the relationship between σ_m and the d with the d less than 50 μm.

We adopted the method of injecting enough negative ions onto the FEP (and Kapton) films surface by an air-ionization-gun when the two electrodes of TENG were separated. The process of ion injection was carried out for several times to realize a high enough surface charge density that can result in air breakdown. Then a sharp decrease of charge density is observed when the electrodes move to contact, indicating air breakdown occurred (Fig. 3a, d). Due to the instantaneity of the air breakdown, the charge density in the first cycle after the sharp decrease could be regarded as the maximum surface charge density. With the thickness of FEP (and Kapton) decreasing, the σ_m has a tendency to increase, which values are consistent with the theoretical analysis (Fig. 3b, e). As a result, the σ_m in air is up to an high value of 1090 μC m^{-2} with an thin Kapton film of 6 μm, and the value of 575 μC m^{-2} for FEP film is achieved at the thickness of 12.5 μm (Figs. S4 and 5). It can be found that the experimental results by ions injection method match well with theoretical curve, except for the relatively thinner Kapton films of 6 μm. This inconsistency may be due to the surface defects increasing with the thickness decreasing, which may result in a higher partial charge density compared to the theoretical value, or the partial micro discharging resulted from the charge diffusion to the back electrode, which is easier for the thin dielectric film.

It should be noted that even though a high charge density can be obtained using thinner Kapton or FEP films, a charge decreasing similar to exponential decay can be observed under high charge density after air breakdown, and then the decay in charge density exhibits slowdown trend with time increasing (Fig. 3c, f and Supplementary Fig. 6). To explain the phenomenon of surface charge decay with time in atmosphere, the decay equation based on charge interface recombination model was established. Firstly, we assume that the amount of initial charges on the dielectric layer surface after air breakdown is Q_I. Due to the large difference of charge polarity between the dielectric layer surface and air, the charges on dielectric layer surface will spontaneously recombine with the particles charged oppositely in air. For the apparent decay of surface charges, it's rational to ignore the effect of triboelectrification, especially during the short time after ion injection. At the time of considering the effect of charges produced by triboelectrification, the corresponding amount of surface charges is defined as Q_T. Hence, only the process of charges decay during the time that surface charges decreased from Q_I to Q_T should be concerned about, wherein the accumulative decayed charges ($\triangle Q_D$) can be written as:

$$\Delta Q_D = Q_I - Q_T \tag{13}$$

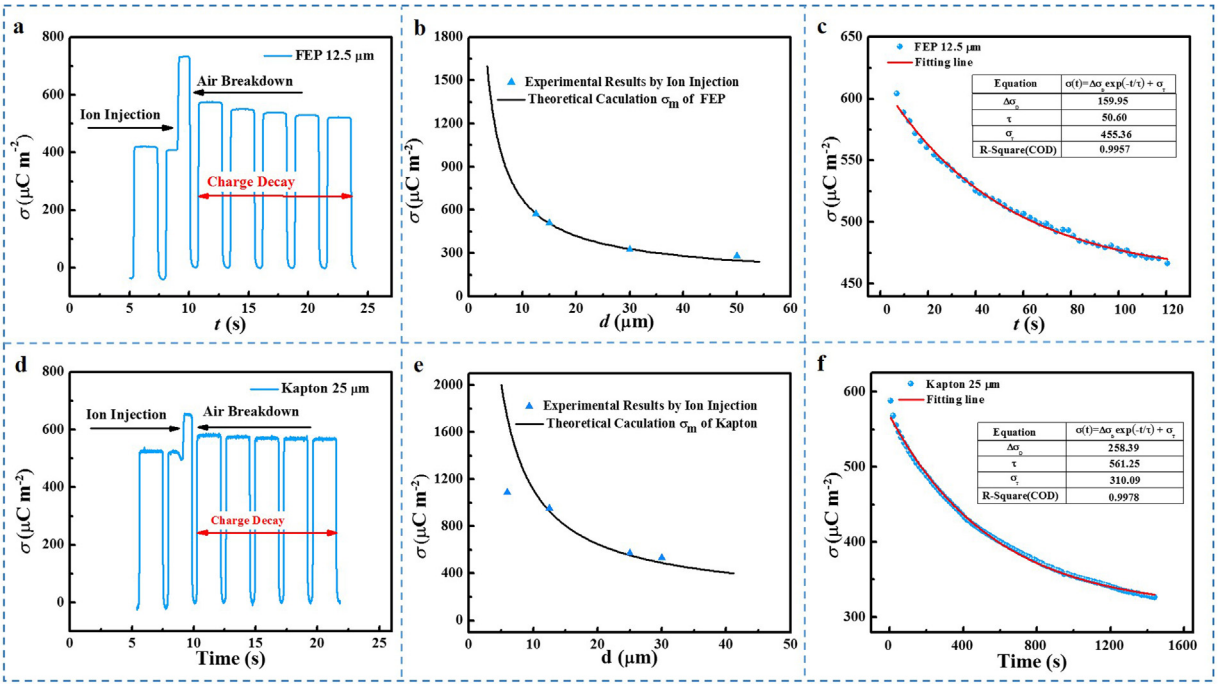

Fig. 3. Output performance of TENG with thin dielectric layer via ion injection method. a) The surface charge density before and after the ions injection during the separation process showing the occurring of air break down; b) Comparison between the charge density of FEP films (12.5, 15, 30 and 50 μm) after ion injection in first cycle and theoretical values. c) The charge decay process on FEP film of 12.5 μm after ions injection. d) The surface charge density before and after the ions injection during the separation process showing the occurring of air break down; e) Comparison between the charge density of Kapton film (6, 12.5, 25, and 30 μm) after ion injection in first cycle and theoretical calculation. f) The charge decay process on Kapton film of 12.5 μm after ions injection. R-Square (COD), coefficient of determination, stands for the proportion of the variance in the dependent variable that is predictable from the independent variable.

To describe the average existing time of dielectric surface charges, it is called the lifetime displayed by τ, then the decay equation can be written as (Supplementary Note 7):

$$\sigma(t) = \Delta\sigma_D \exp\left(-t/\tau\right) + \sigma_T \tag{14}$$

To verify our assumption, the function was applied to fit the experiment values of surface charge density. It should be noted that the dielectric constant of FEP (2.1) is almost the half of Kapton film (4), thus Kapton film with 25 μm and FEP film with 12.5 μm have a similar theoretical σ_m (Supplementary Note 8). Both of their charge decay process shows great consistency with the charge interface recombination model during the time until triboelectrification effect working. The higher σ_T of FEP means that FEP has a better performance of triboelectrification than that of Kapton. This may be a new method to characterize the triboelectrification ability of dielectric material.

2.4. Achieving high surface charge density via triboelectrification

Except introducing the charge by using artificial injection method, the relationship between the surface charge density and dielectric layer thickness below 50 μm was also investigated via triboelectrification process, which can be used to study the charge accumulation process. In this experiment, the mixture of silicon rubber and carbon black instead of the cooper electrode was used as triboelectric electrode for improving contact intimacy [27], meanwhile FEP films with the thicknesses of 12.5, 15, 30, and 50 μm and Kapton films with the thicknesses of 6, 12.5, 15, and 30 μm were served as dielectric layer, respectively. When Kapton film contacted with triboelectric electrode, the surface charges generated and the amount of charges accumulated while the triboelectrification process carried out repeatedly (Fig. 4a). With the further triboelectrification, the charge density gradually tends to be stable and finally reached 303 μC m^{-2} (Fig. S6). Similarly, a stable and high surface charge density of 418 μC m^{-2} was achieved in atmosphere by using FEP film with thickness of 15 μm (Fig. 4d). Compared with the significant charge decay via ion injection method, a stable surface charge density of different thickness of dielectric films is obtained though triboelectrification process. The theory analysis is carried out to elaborate the phenomenon as following. It's widely acknowledged that it takes some time for charges distributing on the surface of dielectric films and then accumulating to saturation step by step. Hence, it's rational for us to assume that there are some charges ΔQ_A transferred from triboelectric electrode to dielectric layer in every cycle, and at the same time, some charges ΔQ_D would decay as described before during the separation process in the air. As a consequence, the effective increasing amount of charges ΔQ_E in every cycle can be defined as Eq. (15):

$$\Delta Q_E = \Delta Q_A - \Delta Q_D \tag{15}$$

When the ΔQ_E is equal to zero, the surface charge density will be saturated. Then, the dynamic equilibrium between charges accumulating and decaying will be established at the same time, resulting in the steady maximized output of TENGs. Therefore, the obtained stable charge density through triboelectrification is derived from the dynamic equilibrium between charge accumulation and decay process.

The surface charge density of Kapton increased to the maximum value with the thickness decrease from 30 to 25 μm, and then declined with the thickness further decrease from 25 to 6 μm (Fig. 4b). Though their surface charge density is far from the theoretical value due to its ordinary triboelectrification performance, it has an improvement than previous work[23]. The similar tendency was observed by using different thickness of FEP films (Fig. 4e). It can be found that the measured datum of FEP (50, 30 and 15 μm) is extremely close to the theoretical value, while the FEP of 12.5 μm shows colossal discrepancies with simulated points (Fig. 4c, f). The unusual phenomenon may be derived from materials defect

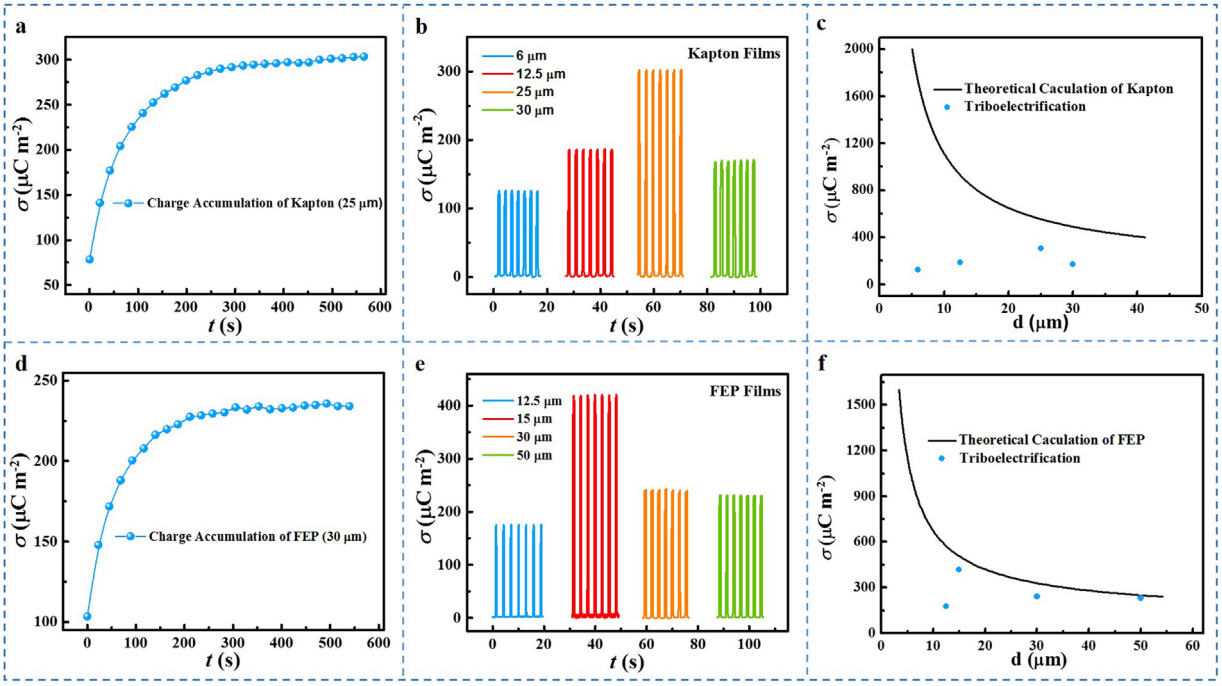

Fig. 4. Output performance of TENG with different thickness of dielectric layer via triboelectrification at frequency of 0.4 Hz. a) Charge accumulation process of Kapton with thickness of 25 μm. b) Surface charge density of Kapton films with thickness of 6, 12.5, 25, and 30 μm via the triboelectrification. c) Theoretical relationship between σ_m and the thickness of Kapton film, with the points of the experimental values. d) Charge accumulation process of FEP with thickness of 30 μm. e) Surface charge density of FEP films with thickness of 12.5, 15, 30, 50 μm via the triboelectrification. f) Theoretical relationship between σ_m and the thickness of FEP film, with the points of the experimental values.

on thinner film surface, which would lead to the imperfect contact between the triboelectric electrode and thin dielectric film, then resulting in the vastly weaken of output performance during triboelectrification process (Figs. S8 and 9). Of course, the exact mechanism needs to be investigated in the future work. On the other hand, the decay process will enhance on the thin films as discussed before. These two hypotheses are confirmed by the phenomena that an high charge density of 1003 μC m^{-2} could be achieved through the charge accumulation on the FEP film of 200 μm in in high vacuum (10^{-6} torr) without the charge decay caused by the charge recombination in the air and without considering the defects in thick dielectric layer [25] (Fig. S10).

From the Fig. 2c, it notes that the σ_m can reach an high theoretical value with a micro separation distance, which is much higher than that with a centimeter separation distance [30]. To demonstrate the theoretical deduction, we design a sliding model TENG (Supplementary Note 8) [34]. A high and stable surface charge density of 735 μCm^{-2} is achieved with an thin FEP film of 15 μm (Fig. S11 and 12), which is much higher than that in CS-TENG. From the Eqs. (9), (10) and Fig. 2d, it can be figured out that a CS-TENG with a FEP film (15 μm) whose maximum surface charge density is 507 μCm^{-2} when the separation distance is over 14.7 μm. There are four reasons why the maximum surface charge density in sliding model TENG is higher than that in CS-TENG. Firstly, if the gap distance between the Cu electrode and dielectric layer is smaller than 14.7 μm, the high charge density can be attained with almost no air breakdown. Furtherly, if the gap distance is smaller than 6.2 μm, which is entirely possible in sliding model TENG, there will be no air breakdown even with a high surface charge density of 735 μC m^{-2}, according to the Eq. (10) and Fig. 2c. In addition, due to the electrostatic shielding of the back electrode, there is almost no air breakdown between the edges of sliding electrode and dielectric layer. More importantly, the S-TENG enhances the triboelectrification effect between the Cu electrode and dielectric layer, so there will be more charges transferred in every cycle than that in CS-TENG, resulting a faster charge accumulation and a higher equilibrium surface charge density according to formula (15).

2.5. Application demonstration of TENG with thin dielectric layer

To further demonstrate the effectivity of adopting thin films, contrast experiments were conducted through driving various electronics by the CS-TENGs with thin FEP films (15 μm) and conventional FEP films (200 μm), named $TENG_{15}$ and $TENG_{200}$, respectively. The simplified self-powered system circuit schematic consists of TENG, a full-wave rectifier and an energy storage unit (a capacitor) (Fig. 5a). When the switch K1 is on and K2 is off, the TENGs were operated at 2 Hz to charge a capacitor of 10 μF. By using $TENG_{15}$, it only takes 41 s to make the voltage of capacitor increase by 9.5 V. As for the $TENG_{200}$, it takes approximately 3-fold time (128 s) for charging the same capacitor (Fig. 5b).

When the switch K1 is off and K2 is on, a capacitor of 47 μF was discharging to drive the electronic watch alone, and the equivalent galvanostatic discharging current (I_{eg}) is 0.61 μA (Supplementary Note 9). When both switch K1 and K2 are on and the TENGs were operated at a low frequency of 3 Hz, the voltage of capacitor is increasing over the time, which means that TENGs can generate more energy than the watch consumes. It can sustainably drive electronic watch and charge the capacitor (Supplementary Movie 1), but the charging current of capacitor with $TENG_{15}$ is 1.74 μA, and that is only 0.78 μA for $TENG_{200}$ (Fig. 5c).

To further verify the effectivity of thin film TENG, a calculator whose energy consumption is higher than that of electronic watch was driven by the TENGs with the same method, where its I_{eg} is 1.41 μA. The voltage of capacitor declined when the $TENG_{200}$ was working, indicating that $TENG_{200}$ couldn't meet the energy consumption of calculator. By contrast, The $TENG_{15}$ can power the calculator and charge the capacitor simultaneously and sustainably, while the charging current is 1.36 μA (Fig. 5d, Supplementary Movie 2).

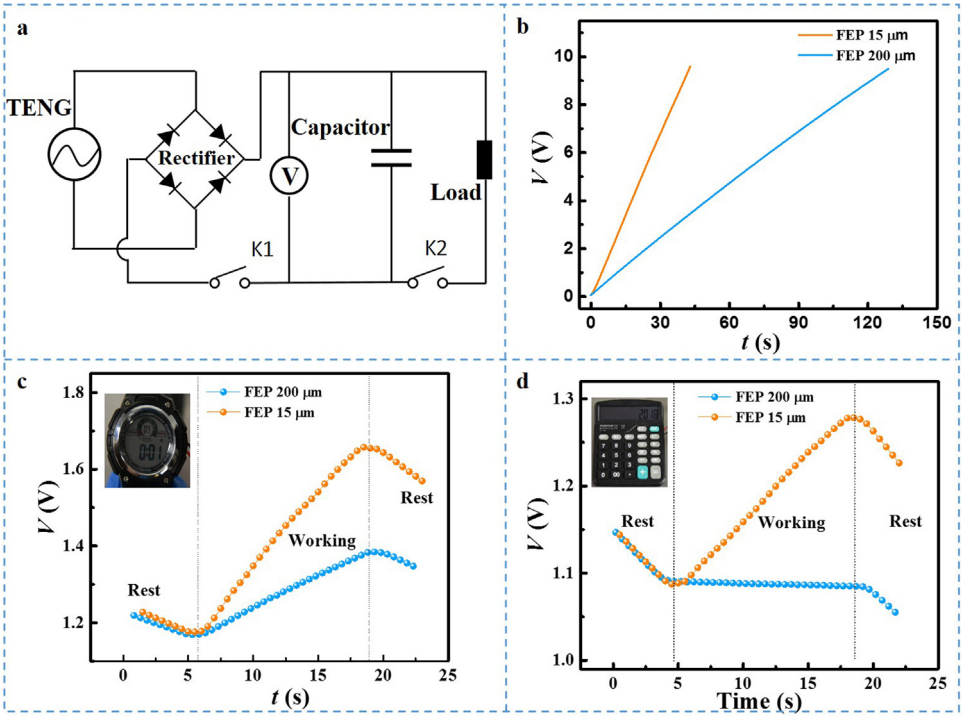

Fig. 5. Application of the TENG with thin dielectric layer to drive electronics devices. a) Circuit schematic of the self-powered system consisting of the TENG and a capacitor. b) Comparison of the charging curves of the capacitor of 10 μF by operating the $TENG_{15}$ and $TENG_{200}$ at 2 Hz. c) An electronic watch is driven and a capacitor of 47 μF is charged simultaneously by $TENG_{15}$ and $TENG_{200}$ at 3 Hz. d) A calculator is driven and a capacitor of 100 μF is charged simultaneously by $TENG_{15}$ but the calculator is driven by $TENG_{200}$ and the capacitor.

3. Conclusions

In this work, we comprehensively rebuilt the basic theory about the limiting factors of maximum surface charge density (σ_m) through mathematical derivation of its limitation equation. It was first to point out the dead zone of Paschen's law in the output performance description of TENG, in which the air gap should be over 3.34 μm. Besides, within the restricted x>9.09 μm, the relationship between the σ_m and the d described by the Eqs. (11) and (12) is workable.

Through the above mathematical derivation, the quantitative relationship σ_m and x_{Sep} is first proposed. With a certain d, the σ_m increases with the x_{Sep} decreasing in the range from 3.34 μm to the distance(x_E) where air breakdown occurs. Therefore, decreasing the x_{Sep} to microscale, the σ_m will be further largely improved, which is verified by the high triboelectric charge density of 735 μC m^{-2} attained in sliding model TENG with a FEP of 15 μm. Furthermore, according to the Eq. (10), it can be figured out that the σ_m can be up to 1100 μC m^{-2} when the x_{Sep} is less than 4.87 μm, which is close to the FEP film dielectric breakdown[25]. These results demonstrate that a higher σ_m can be achieved in micro-nano separation distance, which is also beneficial to the miniaturization and integration of TENG.

Through the mathematical derivation, the quantitative relationship of σ_m and the d is also deduced, which is that σ_m increases with the decreasing of d. By ion injection method, it's demonstrated that the relationship is also suitable for the dielectric layer thinner than 50 μm. And through a charge accumulation process caused by triboelectrification, the charge densities of FEP films (50, 30, and 15 μm) are extremely close to the theoretical value, further confirming the theory. Besides, the validity of thin film also completely verified in the self-charge excitation TENG system, in which a high charge density of 720 μC m^{-2} was attained with a Kapton film of 9 μm[28]. Theoretically, the σ_m can reach 1100 μC m^{-2} with the ultalthin film FEP of 5.32 μm calculated from the Eq. (12). However, further decreasing the thickness of dielectric layer will cause the decline of σ_m, which may be arise from materials defect on thinner film surface. Future work will involve the material optimization to further enhance the surface charge and output performance of TENG.

In summary, our study firstly points out the available range of Paschen's law in TENG field, and then points to effective approaches for enhancing the σ_m of TENGs with micro-nano separation distance or thin films. An high surface charge density was directly obtained through triboelectrification effect in atmosphere. Additionally, the revealed charges accumulation and decay processes will benefit for the fundamental understanding of the triboelectrification effect lasting for thousands of years. Our findings not only establish new optimization methodologies for TENG, but also provide a new perspective of triboelectrification process and triboelectric nanogenerators.

4. Experimental section

4.1. Fabrication of the TENGs

TENGs used in ion injection: a piece of foam was attached to an acrylic substrate, then a Cu film working as an electrode was adhered to the foam. As for the triboelectric dielectric material, a FEP (Kapton) film deposited with a Cu layer via vacuum magnetron sputtering on the bottom was adhered to another acrylic substrate (Fig. S13a). TENGs used in triboelectrification: a piece of silicon rubber-carbon electrode was attached to an acrylic substrate, which detailed preparation method is presented in Supplementary Note 10. As for the triboelectric material, a FEP (Kapton) film deposited with a Cu layer via vacuum magnetron sputtering on the bottom was adhered to another acrylic substrate (Fig. S13b). Mutilayered TENGs: Kapton film with thickness of 130 μm was folded into zigzag with 5 layers, acting as the substrate. Then a Cu film with

an area of 3×5 cm^2 is adhere to the both sides of Kapton film. Then FEP (15 or 200 μm) layers were attached on both sides of Cu layer every other layer. The small dimension TENG with size of 2×2 cm^2 used for studying size effects were fabricated by the same method (Fig. S14).

4.2. Characterization

The short-circuit current and transferred charges were measured by a programmable electrometer (Keithley model 6514). The contact-separation process was implemented by a linear motor (TSMV120-1S). Ionized-air-injection for the introduction of the surface charges was achieved by an air-ionization gun (Milty Zerostat 3). A potentiostat (Bio-Logic VSP-300, France) was utilized to test the capacitance of the capacitor and the charging/discharging curves of the self-charging power system. The microstructures of samples were conducted by a cold field emission scanning electron microscope (FESEM, HITACHI SU8200) with the working voltage and current of 5 kV and 10 μA, respectively.

Declaration of Competing Interest

The authors declared that they have no conflicts of interest to this work.

Acknowledgments

Research supported by the National Key R & D Project from Minister of Science and Technology (2016YFA0202704), National Natural Science Foundation of China (Grant No.61774016, 21773009, 51432005, 5151101243, 51561145021), Beijing Municipal Science & Technology Commission (Z171100000317001, Z171100002017017, Y3993113DF).

Appendix A. Supplementary data

Supplementary material related to this article can be found, in the online version, at doi:https://doi.org/10.1016/j.apmt.2019.100496.

References

[1] S. Chu, A. Majumdar, Nature 488 (2012) 294–303.
[2] J. Chen, Y. Huang, N. Zhang, H. Zou, R. Liu, C. Tao, X. Fan, Z.L. Wang, Nat. Energy 1 (2016) 16138.
[3] F. Fan, Z. Tian, Z.L. Wang, Nano Energy 1 (2012) 328–334.
[4] Z.L. Wang, Faraday Discuss. 176 (2012) 447–458.
[5] Z.L. Wang, Mater. Today 20 (2017) 74–82.
[6] H. Zou, Y. Zhang, L. Guo, P. Wang, X. He, G. Dai, H. Zheng, C. Chen, A.C. Wang, C. Xu, Z.L. Wang, Nat. Commun. 10 (2019) 1427.
[7] C. Wu, A.C. Wang, W. Ding, H. Guo, Z.L. Wang,Adv. Energy Mater. 9 (2019), 1802906.
[8] S. Pan, Z. Zhang,J. Appl. Phys. 122 (2017), 144302.
[9] S. Pan, Z. Zhang, Friction 7 (2019) 2–17.
[10] Q. Zheng, Y. Zou, Y. Zhang, Z. Liu, B. Shi, X. Wang, Y. Jin, H,Sci. Adv. 2 (2016), e1501478.
[11] J. Bae, J. Lee, S. Kim, J. Ha, B.S. Lee, Y. Park, C. Choong, J.B. Kim, Z.L. Wang, H.Y. Kim, J.J. Park, U.I. Chung, Nat. Commun. 5 (2014) 4929.
[12] G. Zhu, J. Chen, T. Zhang, Q. Jing, Z.L. Wang, Nat. Commun. 5 (2014) 3426.
[13] Z.L. Wang, Nature 542 (2017) 159–160.
[14] Y. Zi, L. Lin, J. Wang, S. Wang, J. Chen, X. Fan, P.K. Yang, F. Yi, Z.L. Wang, Adv. Mater. 27 (2015) 2340–2347.
[15] Z. Wen, M.H. Yeh, H. Guo, J. Wang, Y. Zi, W. Xu, J. Deng, L. Zhu, X. Wang, C. Hu, L. Zhu, X. Sun, Z.L. Wang,Sci. Adv. 2 (2016), e1600097.
[16] F. Yi, X. Wang, S. Niu, S. Li, Y. Yin, K. Dai, G. Zhang, L. Lin, Z. Wen, H. Guo, J. Wang, M.H. Yeh, Y. Zi, Q. Liao, Z. You, Y. Zhang, Z.L. Wang,Sci. Adv. 2 (2016), eaat2516.
[17] X. Pu, H. Guo, J. Chen, X. Wang, Y. Xi, C. Hu, Z.L. Wang,Sci. Adv. 3 (2017), e1700694.
[18] H. Guo, X. Pu, J. Chen, Y. Meng, M.H. Yeh, G. Liu, Q. Tang, B. Cheng, D. Liu, S. Qi, C. Wu, C. Hu, J. Wang, Z.L. Wang,Sci. Robot. 3 (2018), eaat2516.
[19] J. Wang, X. Li, S. Wang, Z. Li, L. Zheng, F. Yi, S. Li, Z.L. Wang, Adv. Mater. 27 (2015) 4830–4836.
[20] Y. Zi, S. Niu, J. Wang, Z. Wen, W. Tang, Z.L. Wang, Nat. Commun. 6 (2015) 8376.
[21] J. Peng, S.D. Kang, G.J. Snyder,Sci. Adv. 3 (2017), eaap8576.
[22] J. Zhong, Q. Zhong, F. Fan, Y. Zhang, S. Wang, B. Hu, Z.L. Wang, J. Zhou, Nano Energy 2 (2013) 491–497.
[23] N. Cui, L. Gu, Y. Lei, J. Liu, Y. Qin, X. Ma, Y. Hao, Z.L, ACS Nano 10 (2016) 6131–6138.
[24] J. Wang, Z. Wen, Y. Zi, P. Zhou, J. Lin, H. Guo, Y. Xu, Z.L. Wang, Adv. Funct. Mater. 26 (2016) 1070–1076.
[25] S. Wang, Y. Zi, Y. Zhou, S. Li, F. Fan, L. Lin, Z.L. Wang, J. Mater. Chem. A 4 (2016) 3728–3734.
[26] S. Wang, Y. Xie, S. Niu, L. Lin, C. Liu, Y. Zhou, Z.L. Wang, Adv. Mater. 26 (2014) 6720–6728.
[27] J. Wang, S. Li, F. Yi, Y. Zi, J. Lin, X. Wang, Y. Xu, Z.L. Wang, Nat. Commun. 7 (2016) 12744.
[28] Y. Zi, C. Wu, W. Ding, Z.L. Wang,Adv. Funct. Mater. 27 (2017), 1700049.
[29] J. Wang, C. Wu, Y. Dai, Z. Zhao, A. Wang, T. Zhang, Z.L. Wang, Nat. Commun. 8 (2017) 88.
[30] L. Xu, T.Z. Bu, X.D. Yang, C. Zhang, Z.L. Wang, Nano Energy 49 (2018) 625–633.
[31] L. Cheng, Q. Xu, Y. Zheng, X. Jia, Y. Qin, Nat. Commun. 9 (2018) 3773.
[32] W.Z. Liu, G. Wang, G. Wang, J. Liu, X. Chen, Y. Pu, X. Xi, H. Wang, C. Guo, Z. Hu, L. Wang, Nat. Commun. 10 (2019) 1426.
[33] K.T.A.L. Burm, Contrib. Plasma Phys. 47 (2007) 177–182.
[34] S. Niu, S. Wang, L. Lin, Y. Liu, Y. Zhou, Y. Hu, Z.L. Wang, Energy Environ. Sci. 6 (2013) 3576.